BRAIN
A JOURNAL OF NEUROLOGY

REPORT

Identifying the ischaemic penumbra using pH-weighted magnetic resonance imaging

George W. J. Harston,[1] Yee Kai Tee,[2,3] Nicholas Blockley,[4] Thomas W. Okell,[4] Sivarajan Thandeswaran,[1] Gabriel Shaya,[1] Fintan Sheerin,[5] Martino Cellerini,[5] Stephen Payne,[2] Peter Jezzard,[4] Michael Chappell[2] and James Kennedy[1]

The original concept of the ischaemic penumbra suggested imaging of regional cerebral blood flow and metabolism would be required to identify tissue that may benefit from intervention. Amide proton transfer magnetic resonance imaging, a chemical exchange saturation transfer technique, has been used to derive cerebral intracellular pH in preclinical stroke models and has been proposed as a metabolic marker of ischaemic penumbra. In this proof of principle clinical study, we explored the potential of this pH-weighted magnetic resonance imaging technique at tissue-level. Detailed voxel-wise analysis was performed on data from a prospective cohort of 12 patients with acute ischaemic stroke. Voxels within ischaemic core had a more severe intracellular acidosis than hypoperfused tissue recruited to the final infarct ($P < 0.0001$), which in turn was more acidotic than hypoperfused tissue that survived ($P < 0.0001$). In addition, when confined to the grey matter perfusion deficit, intracellular pH ($P < 0.0001$), but not cerebral blood flow ($P = 0.31$), differed between tissue that infarcted and tissue that survived. Within the presenting apparent diffusion coefficient lesion, intracellular pH differed between tissue with early apparent diffusion lesion pseudonormalization and tissue with true radiographic recovery. These findings support the need for further investigation of pH-weighted imaging in patients with acute ischaemic stroke.

1 Acute Stroke Programme, Radcliffe Department of Medicine, University of Oxford, UK
2 Institute of Biomedical Engineering, Department of Engineering Science, University of Oxford, UK
3 Department of Mechatronics and Biomedical Engineering, Lee Kong Chian Faculty of Engineering and Science, Universiti Tunku Abdul Rahman, Malaysia
4 Oxford Centre for Functional MRI of the Brain, Nuffield Department of Clinical Neurosciences, University of Oxford, UK
5 Department of Neuroradiology, Oxford University Hospitals NHS Trust, Oxford, UK

Correspondence to: Dr James Kennedy,
Acute Vascular Imaging Centre, University of Oxford, Level 2,
John Radcliffe Hospital, Headington, Oxford, OX3 9DU, UK
E-mail: james.kennedy@rdm.ox.ac.uk

Introduction

The original concept of the ischaemic penumbra suggested that concurrent imaging of regional cerebral blood flow (CBF) and metabolism would be required to identify tissue at risk that may benefit from intervention (Astrup et al., 1981). Although there have been major technological advances in acute stroke imaging since this was proposed, the search for robust evidence to support individual imaging-guided treatment decisions is ongoing (Kidwell, 2013; Wintermark et al., 2013). A contributing factor may be that, aside from PET imaging, the development of

Table 1 Patient characteristics

Patient	Stroke syndrome	Hemisphere	Sex	Age	NIHSS	Thrombolysed	Onset to scan, (h:min)	24 h MRI	Follow-up MRI (days)
1	LACS	Left	F	84	3	N	03:25	Y	1 month (37)
2	TACS	Left	M	92	25	Y	02:50	Y	1 week (7)
3	PACS	Right	M	64	3	N	01:41	Y	1 month (37)
4	POCS	Left	M	80	3	N	11:06	N	1 month (37)
5	TACS	Left	F	86	27	N	03:09	Y	1 month (25)
6	TACS	Left	F	81	21	N	03:25	Y	1 week (4)
7	PACS	Left	M	95	19	Y*	04:14	Y	1 month (47)
8	TACS	Left	F	53	13	Y	02:48	Y	1 month (34)
9	LACS	Right	M	57	7	N	01:43	Y	1 month (67)
10	TACS	Right	F	79	14	Y*	09:50	N	1 month (27)
11	PACS	Left	F	78	9	Y	02:50	Y	NA
12	PACS	Left	F	55	7	Y	01:35	Y	1 month (31)

NIHSS = National Institute for Health Stroke Scale; LACS = lacunar stroke; TACS = total anterior circulation stroke; PACS = partial anterior circulation stroke; POCS = posterior circulation stroke; NA = not available.

*Patients 7 and 10 received thrombolysis prior to the MRI scan rather than during it. Patient 7 finished thrombolysis immediately prior to imaging. Patient 10 was imaged 6 h after thrombolysis.

metabolic imaging markers has been limited when compared to the focus on methods to assess perfusion.

Cerebral intracellular pH is maintained until CBF drops to levels associated with irreversible infarction (Hossmann, 1994). Amide proton transfer MRI, a chemical exchange saturation transfer imaging technique, can be used to generate a pH-weighted imaging signal through the assessment of the base-catalyzed and, hence, pH-dependent intracellular transfer of protons between amide groups and water (Zhou *et al.*, 2003). It has been proposed that pH-weighted imaging may improve the delineation of tissue at risk by separating benign oligaemia from an acidotic ischaemic penumbra (Zhou and van Zijl, 2011). Preclinical studies have supported this potential as a biomarker of the ischaemic penumbra (Cho *et al.*, 2007; Sun *et al.*, 2007, 2011), but to date the limited clinical application of pH-weighted imaging has not systematically demonstrated its potential in patients exclusively with acute stroke (Sun *et al.*, 2010; Zhao *et al.*, 2011; Tee *et al.*, 2014; Tietze *et al.*, 2014).

Using detailed voxel-wise analysis to understand tissue-level effects, this proof of principle clinical study assesses the relationship between intracellular pH and final tissue outcome in data from a prospective cohort of patients with acute ischaemic stroke. In doing so, this study explores how pH-weighted imaging may be used in conjunction with the established acute stroke imaging modalities, diffusion and perfusion weighted imaging, to define the ischaemic penumbra.

Materials and methods

Patients

Patients presenting with ischaemic stroke within 12 h of symptom onset (using the last seen well principle) regardless of age or stroke severity were recruited into a prospective observational cohort study following informed consent or agreement from a representative according to protocols approved by UK National Research Ethics Service committees (ref: 12/SC/0292 and 13/SC/0362). Exclusion criteria included the presence of a contraindication for MRI and a diffusion weighted imaging or arterial spin labelling perfusion weighted imaging (ASL-PWI) lesion < 5 mm in axial diameter. MRI was performed at presentation, 24 h, 1 week, and 1 month. All clinical decisions, for example to thrombolyze the patient if indicated, were made prior to enrolment in order not to introduce any delay to best clinical care. The research scanning often took place while thrombolysis was taking place (Table 1).

Image acquisition

A Siemens 3 T Verio scanner was used at all time points. Scanning protocols included diffusion weighted imaging (three directions, $1.8 \times 1.8 \times 2.0$ mm, field of view = 240 mm, four averages, b = 0 and 1000 s/mm^2, repetition time = 9000 ms, echo time = 98 ms, 50 slices, 2 min 53 s) with apparent diffusion coefficient (ADC) calculation; T_1-weighted MP-RAGE ($1.8 \times 1.8 \times 1.0$ mm, field of view = 228 mm, repetition time = 2040 ms, echo time = 4.55 ms, inversion time = 900 ms, 3 min 58 s); vessel-encoded pseudocontinuous ASL-PWI ($3.4 \times 3.4 \times 4.5$ mm, field of view = 220 mm, repetition time = 4080 ms, echo time = 14 ms, echo planar imaging, 24 slices, 5 min 55 s) with multiple post-labelling delays (six delays: 0.25 s, 0.5 s, 0.75 s, 1 s, 1.25 s, 1.5 s) (Okell *et al.*, 2013); and T_2-weighted FLAIR turbo spin echo ($1.9 \times 1.9 \times 2.0$ mm, field of view = 240 mm, repetition time = 9000 ms, echo time = 96 ms, inversion time = 2500 ms). pH-weighted images were acquired by estimating amide proton transfer effect using single-slice chemical exchange saturation transfer echo planar imaging localized to the lesion on diffusion weighted imaging ($3.0 \times 3.0 \times 5.0$ mm, field of view = 240 mm, repetition time = 5000 ms, echo time = 28 ms, echo planar imaging, 1 slice, 2 min 45 s). The chemical exchange saturation transfer preparation consisted of a 2 s train of 50 Gaussian pulses (flip angle = 184°, power = 0.55 µT, duration = 20 ms, delay time = 20 ms) over 32

frequency offsets with an optimized sampling schedule from -4.5 to 4.5 ppm (Tee *et al.*, 2013, 2014).

Postprocessing

All image analysis was performed using FSL (Jenkinson *et al.*, 2012) and MATLAB (The Mathworks Inc.). Following brain extraction and automated tissue segmentation of the T_1-weighted image to define grey matter, white matter and CSF, registration within participants used a six degrees-of-freedom rigid body linear transformation to the T_1-weighted image (Zhang *et al.*, 2001; Jenkinson *et al.*, 2002; Smith, 2002). ASL-PWI was processed using a non-linear fit to the general arterial spin labelling (ASL) kinetic model for all voxels within a brain mask to quantify CBF (Chappell *et al.*, 2010; Okell *et al.*, 2013). Perfusion maps were registered to the T_1-weighted image as above. pH-weighted imaging was retrospectively motion corrected using the MCFLIRT tool, registered to the first slice acquired (Jenkinson *et al.*, 2002). pH-weighted signal was quantified using amide proton transfer ratio (APTR*) (Chappell *et al.*, 2013; Tee *et al.*, 2014) where low values represent intracellular acidosis. pH-weighted images were then co-registered with the corresponding T_1-weighted image slice, to which it was aligned at the time of acquisition, using the 2D registration schedule within FSL (Jenkinson *et al.*, 2012) and checked for accuracy by a clinician.

Amide proton transfer ratio analysis

APTR* is a metric combining the effect of amide-proton exchange rate, which is directly related to pH, and relative concentration of amide-bearing molecules. APTR* does not rely upon data from saturation frequencies on the opposite site of the water resonance as a reference unlike conventional APTR, avoiding changes that might occur in ischaemia unrelated to pH, such as B_0 inhomogeneity (Chappell *et al.*, 2013). APTR* has been found to be more homogenous than APTR in healthy subjects and acute stroke patients producing better contrast-to-noise ratio between ischaemic and normal tissue (Tee *et al.*, 2014).

APTR* is derived from model-based analysis of the amide proton transfer z-spectrum and controls for the effects of B_0 inhomogeneity, T_1 and T_2. APTR* is calculated using the fitted model parameters from a three-pool exchange model; APTR* = $[S_w(3.5\,ppm) - S_{w+a}(3.5\,ppm)] / M_{w0}$, where S refers to the simulated signal at 3.5 ppm using the fitted model parameters, subscripts w and w + a refer to water pool and both water and amide pools, and M_{w0} is the fitted unsaturated signal. The three-pool exchange model used for the data fitting was water, amide and asymmetry magnetization transfer. The third pool represents a combination of the saturation effect observed at the negative frequency offsets and the conventional magnetization transfer (Hua *et al.*, 2007; Chappell *et al.*, 2013).

Regions of interest

Binary masks of presenting and 24-h ADC lesions (ADC_0 and ADC_{24}) were automatically generated using a threshold-defined (620×10^{-6} mm^2/s) (Purushotham *et al.*, 2013) cluster-based analysis of the ADC data. Presenting perfusion deficits were defined using a threshold of 20 ml/100 g/min to guide delineation of the region (Bristow *et al.*, 2005). Both ADC and perfusion region of interest clusters were identified and smoothed [Gaussian kernel of standard deviation 1 mm (ADC) and 2 mm (perfusion)], followed by repeat cluster analysis (http://fsl.fmrib.ox.ac.uk/fsl/fslwiki/Cluster). The automated ADC and perfusion masks were inspected to ensure their accuracy and manually corrected when necessary. Final infarct was preferentially defined manually on the 1-month FLAIR image, or, if not available, on the 1-week image. Non-linear registration was used to register the 1-week images to the presenting T_1-weighted image to minimize any overestimation of final FLAIR infarct due to any oedema still present at this time (Jenkinson *et al.*, 2012; Rekik *et al.*, 2012). A representative contralateral region of interest was defined manually on the FLAIR image and blind to the processed APTR* data.

The following tissue outcome definitions were used in the analysis: (i) ischaemic core: tissue present in both ADC_0 and final FLAIR infarct; (ii) infarct growth: tissue present in the final FLAIR infarct but not in the ADC_0; (iii) oligaemia: tissue present in the perfusion deficit but not the final FLAIR infarct; (iv) diffusion lesion pseudonormalization: tissue present in the ADC_0 but not ADC_{24}; that is present in the final FLAIR infarct; and (v) radiographic recovery: tissue present in the ADC_{24} but not the final FLAIR infarct (Supplementary Fig. 1).

Data extraction and analysis

Voxel-wise analysis was used to calculate mean presenting APTR* for each region of interest mask transformed to native amide proton transfer image space within a tissue mask. To enable the secondary analysis of comparing presenting APTR*, grey matter perfusion and ADC directly, APTR*, CBF and ADC were co-registered to T_1-weighted image space. Data were extracted from the regions of interest within a grey matter mask. APTR*, CBF and ADC were calculated relative to the contralateral region of interest enabling composite voxel-wise analysis across patients. Statistical tests used were unpaired *t*-tests for direct comparison between the means in the regions of interest and using ANOVA for multiple region of interest comparisons.
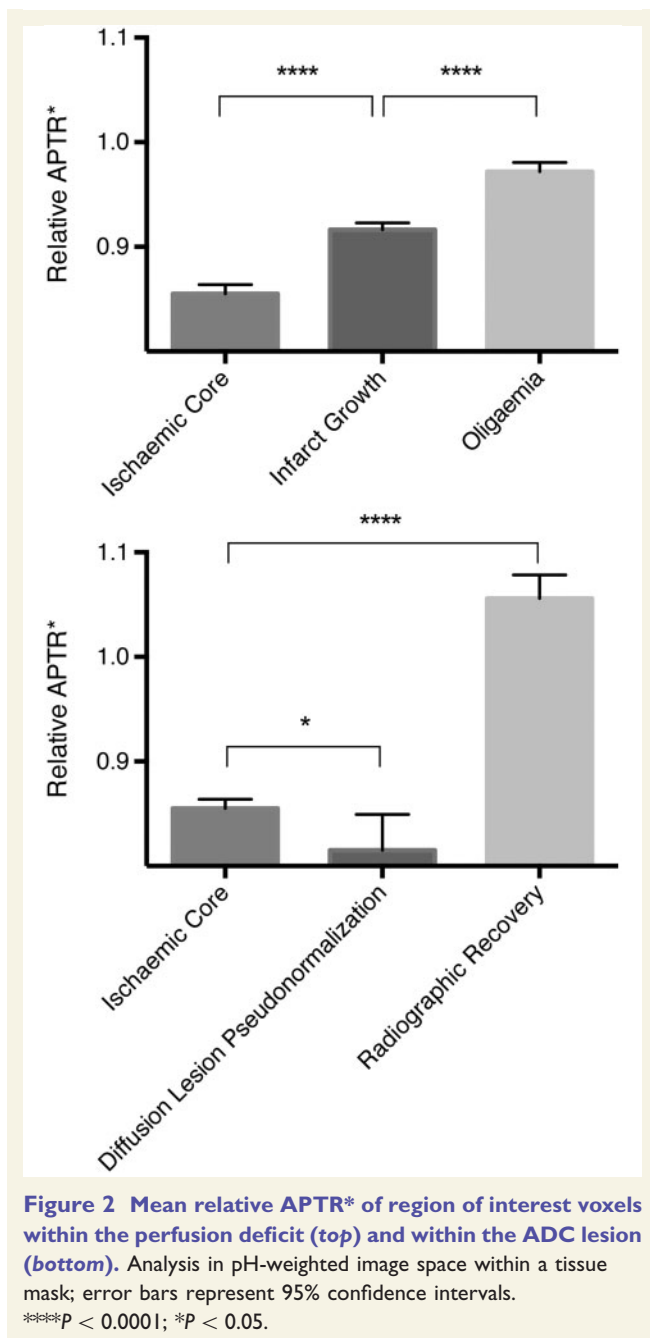
Results

Of 18 eligible patients recruited, 12 were included in the analysis (Table 1). Three patients were excluded because of motion corruption, two because of artefact in the APTR* images (ringing and partial volume effects) and one developed secondary haemorrhage during the initial MRI. The median symptom onset to MRI was 2 h 59 min (range 1 h 35 min to 11 h 6 min) and the median National Institute for Health Stroke Scale at presentation was 11 (minimum: 3, maximum: 27). Six patients received intravenous thrombolysis. Images from representative patients are presented in Fig. 1.

Tissue in ischaemic core, infarct growth and oligaemia regions of interest all demonstrated a reduced APTR* relative to the contralateral hemisphere [mean ± standard deviation (number of voxels); ischaemic core: 0.86 ± 0.11 (636); infarct growth: 0.92 ± 0.11 (912); oligaemia:
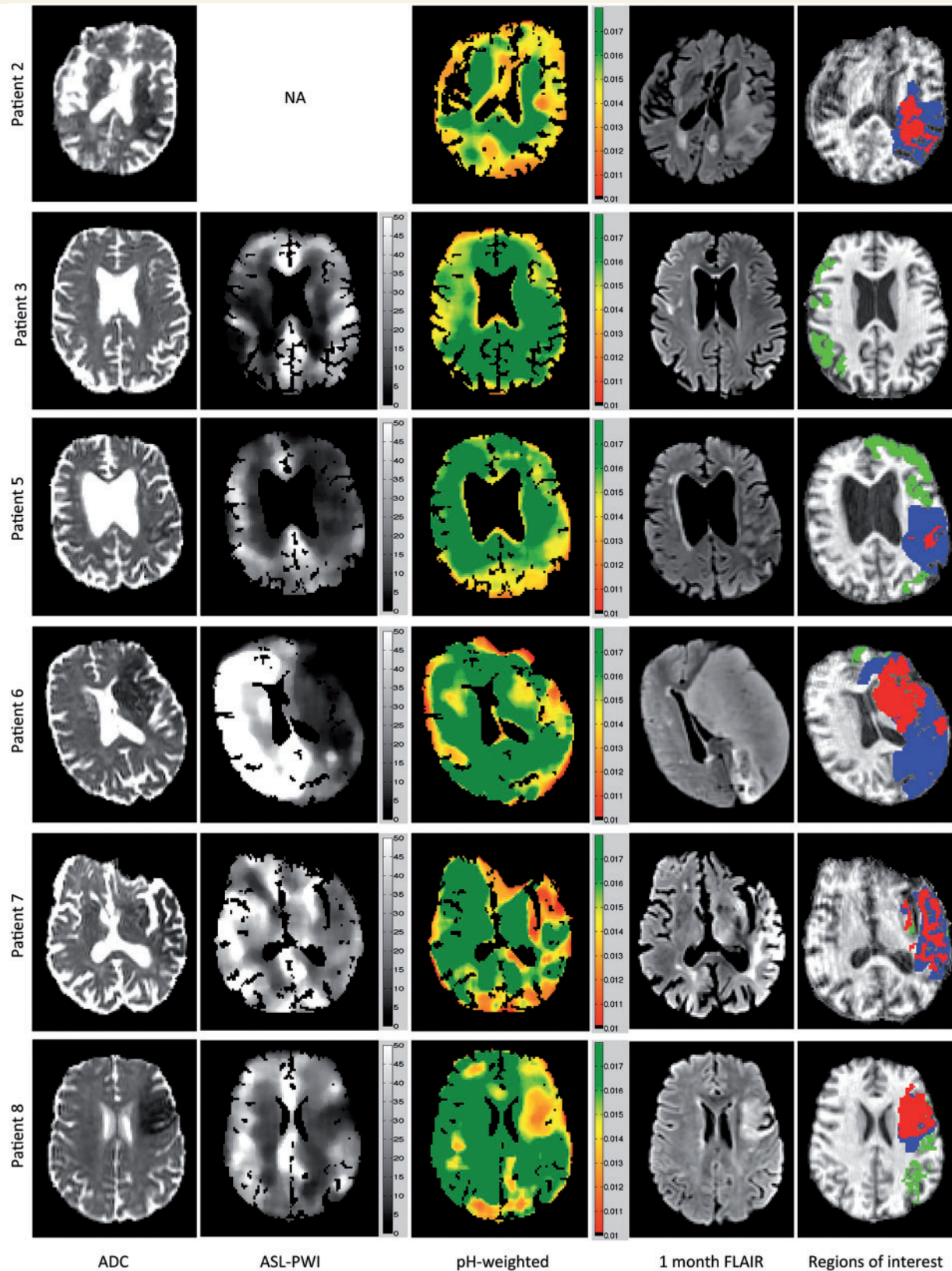
Figure 1 Images from representative patients. Regions of interest: green = oligaemia; blue = infarct growth; red = ischaemic core. NA = not available. Scale for ASL-PWI = cerebral blood flow, ml/100g/min. Scale for pH-weighted imaging = APTR*, no units.

Figure 2 Mean relative APTR* of region of interest voxels within the perfusion deficit (*top*) and within the ADC lesion (*bottom*). Analysis in pH-weighted image space within a tissue mask; error bars represent 95% confidence intervals.
****$P < 0.0001$; *$P < 0.05$.

Figure 3 Mean relative CBF (*top*) and relative APTR* (*bottom*) for region of interest voxels within the perfusion deficit, restricted to grey matter voxels only. Analysis in T_1-weighted image space within a grey matter mask; error bars represent 95% confidence intervals. ****$P < 0.0001$.

0.97 ± 0.11 (592)] (Fig. 2 and Supplementary Table 1). Relative APTR* within the ischaemic core was significantly lower than within the infarct growth voxels ($P < 0.0001$, unpaired *t*-test), which in turn had lower relative APTR* than oligaemia regions ($P < 0.0001$, unpaired *t*-test). Data from individual patients in Fig. 1 can be seen in Supplementary Fig. 2.

Those voxels within the ADC lesions that demonstrated diffusion lesion pseudonormalization [0.82 ± 0.12 (47) had significantly lower relative APTR* than the ischaemic core (0.86 ± 0.11 (636), $P = 0.03$, unpaired *t*-test] (Fig. 2). In contrast, those regions undergoing radiographic recovery had an APTR* greater than the contralateral hemisphere
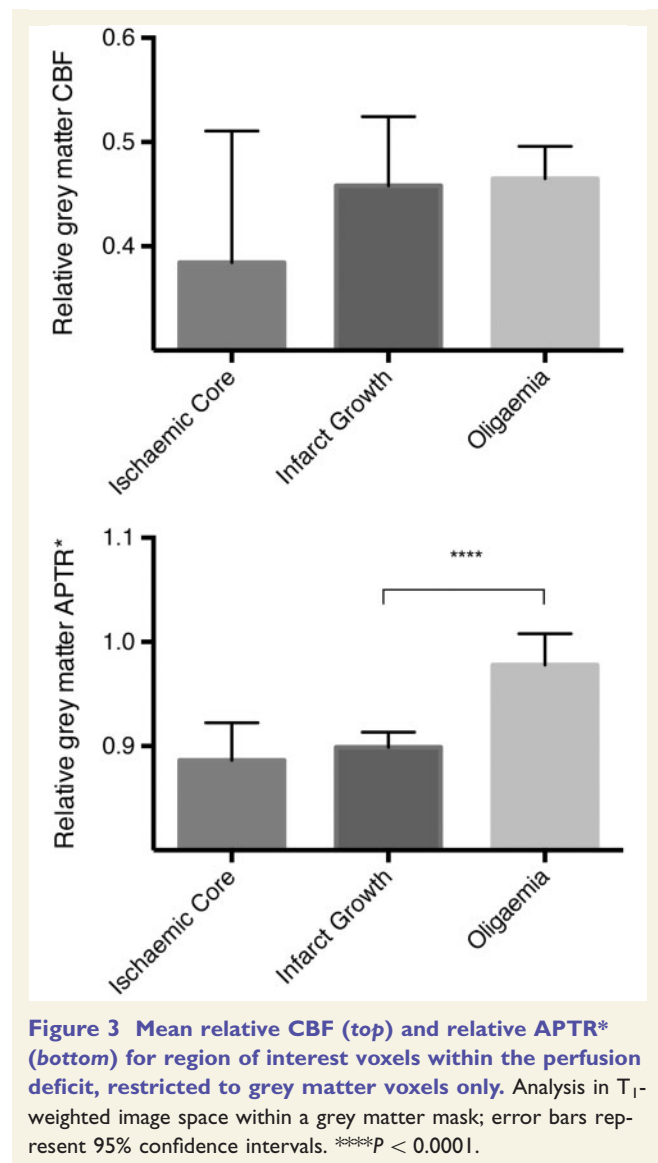
[1.06 ± 0.13 (129)] (Fig. 2). Within the ADC lesions, there was a gradation of mean ADC by final tissue outcome (Supplementary Fig. 3).

Within the grey matter, CBF did not distinguish between regions of ischaemic core, infarct growth or oligaemia ($P = 0.31$, ANOVA) although there was more variation in CBF within the ischaemic core than infarct growth regions (variance ratio = 2.5, $P < 0.01$) (Fig. 3 and Supplementary Fig. 4). In contrast, there was a significant difference in relative APTR* between regions of infarct growth and oligaemia within the grey matter ($P < 0.0001$, unpaired *t*-test), and although the relative APTR* within the ischaemic core was lower than the regions of infarct growth, this was not significant ($P = 0.52$). With the perfusion deficit, the relative ADC value was reduced only in the ischaemic core (Supplementary Fig. 4).

Discussion

Using detailed group-level voxel-wise analysis we demonstrate the potential clinical use of pH-weighted MRI in acute ischaemic stroke. This study builds on previous work to optimize the generation of a pH-weighted signal to show that intracellular pH at presentation is significantly associated with final tissue outcome, providing complementary information to existing ASL-PWI and diffusion weighted imaging sequences in the clinical setting of acute stroke (Sun *et al.*, 2010; Zhao *et al.*, 2011; Tee *et al.*, 2014; Tietze *et al.*, 2014). It entails the use of a sequence acquisition that is clinically pragmatic (it is 3 min in duration), and does not require contrast (e.g. gadolinium) or exogenous stimulus (e.g. inhaled gas such as carbogen) to derive a signal that is present in both grey and white matter (Tee *et al.*, 2014).

This study shows a biologically plausible signal of intracellular acidosis associated with final tissue outcome. Intracellular acidosis develops in part as a consequence of unopposed anaerobic ATP hydrolysis, with hypoperfusion and reduced bicarbonate buffering at acidic pH exacerbating the acidosis (Sun *et al.*, 2011). Within a perfusion-defined lesion, the ischaemic core is more acidotic than tissue that is subsequently recruited to the final infarct. Tissue within the region of interest of oligaemia that ultimately does not infarct is significantly less acidotic than either ischaemic core or infarct growth.

The inherently low signal-to-noise ratio when using ASL to measure CBF in white matter (van Gelderen *et al.*, 2008; Alsop *et al.*, 2014), alongside the sensitivity of ASL to delays in arterial arrival time, provide challenges in the accurate determination of the perfusion deficit and may affect reliable determination of CBF. This was overcome, in part, by the use of multiple post-labelling delays (Okell *et al.*, 2013). Furthermore, when comparing pH-weighted imaging to ASL-PWI within the regions of interest representing different tissue outcomes, analysis was confined to grey matter to minimize any insensitivity introduced by ASL-PWI. Within threshold-defined ischaemic grey matter, pH-weighted imaging, but not ASL-PWI, differed between tissues with different outcomes. Outside of the ischaemic core, relative ADC values were not helpful in discriminating final tissue outcome. This supports the hypothesis that pH-weighted imaging separates the diffusion-perfusion mismatch into zones of acidotic ischaemic penumbra (low CBF with evidence of metabolic stress) and benign oligaemia (low CBF with minimal evidence of metabolic stress) in a way consistent with the preclinical data (Sun *et al.*, 2007; Zhou and van Zijl, 2011).

pH-weighted MRI provides an insight into ADC lesion reversal, which has variously been reported at 6.7% to 50% of the presenting ADC lesion (Inoue *et al.*, 2014). This study corroborates the PET imaging finding that there is heterogeneity of metabolism within the ADC lesion and that this seems to be linked to ADC reversal (Guadagno *et al.*, 2006). Tissue within regions of diffusion lesion pseudonormalization is more severely acidotic at presentation than the ischaemic core, consistent with more aggressive tissue injury with vasogenic oedema and early pseudonormalization of ADC by 24 h (Inoue *et al.*, 2014). In contrast, tissue with radiographic recovery has an intracellular alkalosis. This is again a biologically plausible signature of tissue maintaining ATP levels, and hence viability, through the transfer of phosphate from phosphocreatine to ADP (adenosine diphosphate) with resultant intracellular alkalosis (Erecinska and Silver, 1989).

Further technical development, such as 3D image acquisition to overcome challenges pertaining to single-slice data (including registration errors), rapid image analysis and improving signal-to-noise ratio, is required before pH-weighted imaging becomes a widely clinically relevant imaging modality influencing treatment decisions for individuals. In keeping with other acute stroke MRI modalities, further work is required to limit issues related to motion corruption and partial volume effects. Addressing these will enable larger studies to assess the interaction of the pH-weighted signal with physiological (e.g. glucose, temperature), treatment, and imaging (e.g. perfusion dynamics) parameters.

In conclusion, pH-weighted imaging may have a role in improving the imaging definition of ischaemic penumbra, and may also be useful in a better understanding of regional vulnerability and secondary injury, addressing an unmet need of MRI biomarkers in acute stroke (Kidwell, 2013). In addition, given pH is a physiological parameter that can be manipulated, pH-weighted imaging has the potential to meet the criteria of a treatment-relevant acute imaging target (Wintermark *et al.*, 2013). This proof of principle study at a tissue level of analysis strongly supports the further investigation of pH-weighted imaging in patients with acute ischaemic stroke when used in combination with diffusion and perfusion weighted imaging.

Supplementary material

Supplementary material is available at *Brain* online.

Conflict of interest

Professor Chappell, Professor Jezzard and Dr Okell have received royalties from Siemens Healthcare through licensing of US patents. Professor Chappell has received royalties for commercial licenses from the FMRIB software library.

References

Alsop DC, Detre JA, Golay X, Gunther M, Hendrikse J, Hernandez-Garcia L, et al. Recommended implementation of arterial spin-labeled perfusion MRI for clinical applications: a consensus of the ISMRM perfusion study group and the European consortium for ASL in dementia. Magn Reson Med. Advance Access published on April 8, 2014, doi: 10.1002/mrm.25197.

Astrup J, Siesjo BK, Symon L. Thresholds in cerebral ischemia - the ischemic penumbra. Stroke 1981; 12: 723–5.

Bristow MS, Simon JE, Brown RA, Eliasziw M, Hill MD, Coutts SB, et al. MR perfusion and diffusion in acute ischemic stroke: human gray and white matter have different thresholds for infarction. J Cereb Blood Flow Metab 2005; 25: 1280–7.

Chappell MA, Donahue MJ, Tee YK, Khrapitchev AA, Sibson NR, Jezzard P, et al. Quantitative bayesian model-based analysis of amide proton transfer MRI. Magn Reson Med 2013; 70: 556–67.

Chappell MA, Okell TW, Jezzard P, Woolrich MW. A general framework for the analysis of vessel encoded arterial spin labeling for vascular territory mapping. Magn Reson Med 2010; 64: 1529–39.

Cho SH, Kim DG, Kim DS, Kim YH, Lee CH, Jang SH. Motor outcome according to the integrity of the corticospinal tract determined by diffusion tensor tractography in the early stage of corona radiata infarct. Neurosci Lett 2007; 426: 123–7.

Erecinska M, Silver IA. ATP and brain function. J Cereb Blood Flow Metab 1989; 9: 2–19.

Guadagno JV, Warburton EA, Jones PS, Day DJ, Aigbirhio FI, Fryer TD, et al. How affected is oxygen metabolism in DWI lesions?: a combined acute stroke PET-MR study. Neurology 2006; 67: 824–9.

Hossmann KA. Viability thresholds and the penumbra of focal ischemia. Ann Neurol 1994; 36: 557–65.

Hua J, Jones CK, Blakeley J, Smith SA, van Zijl PC, Zhou J. Quantitative description of the asymmetry in magnetization transfer effects around the water resonance in the human brain. Magn Reson Med 2007; 58: 786–93.

Inoue M, Mlynash M, Christensen S, Wheeler HM, Straka M, Tipirneni A, et al. Early diffusion-weighted imaging reversal after endovascular reperfusion is typically transient in patients imaged 3 to 6 hours after onset. Stroke 2014; 45: 1024–8.

Jenkinson M, Bannister P, Brady M, Smith S. Improved optimization for the robust and accurate linear registration and motion correction of brain images. Neuroimage 2002; 17: 825–41.

Jenkinson M, Beckmann CF, Behrens TE, Woolrich MW, Smith SM. FSL. Neuroimage 2012; 62: 782–90.

Kidwell CS. MRI biomarkers in acute ischemic stroke: a conceptual framework and historical analysis. Stroke 2013; 44: 570–8.

Okell TW, Chappell MA, Kelly ME, Jezzard P. Cerebral blood flow quantification using vessel-encoded arterial spin labeling. J Cereb Blood Flow Metab 2013; 33: 1716–24.

Purushotham A, Campbell BC, Straka M, Mlynash M, Olivot JM, Bammer R, et al. Apparent diffusion coefficient threshold for delineation of ischemic core. Int J Stroke. Advance Access published on June 27, 2013, doi: 10.1111/ijs.12068.

Rekik I, Allassonniere S, Carpenter TK, Wardlaw JM. Medical image analysis methods in MR/CT-imaged acute-subacute ischemic stroke lesion: segmentation, prediction and insights into dynamic evolution simulation models. A critical appraisal. NeuroImage Clin 2012; 1: 164–78.

Smith SM. Fast robust automated brain extraction. Human Brain Mapp 2002; 17: 143–55.

Sun PZ, Benner T, Copen WA, Sorensen AG. Early experience of translating pH-weighted MRI to image human subjects at 3 tesla. Stroke 2010; 41: S147–51.

Sun PZ, Cheung JS, Wang E, Lo EH. Association between pH-weighted endogenous amide proton chemical exchange saturation transfer MRI and tissue lactic acidosis during acute ischemic stroke. J Cereb Blood Flow Metab 2011; 31: 1743–50.

Sun PZ, Zhou J, Sun W, Huang J, van Zijl PC. Detection of the ischemic penumbra using pH-weighted MRI. J Cereb Blood Flow Metab 2007; 27: 1129–36.

Tee YK, Harston GW, Blockley N, Okell TW, Levman J, Sheerin F, et al. Comparing different analysis methods for quantifying the MRI amide proton transfer (APT) effect in hyperacute stroke patients. NMR Biomed 2014; 27: 1019–29.

Tee YK, Khrapitchev AA, Sibson NR, Payne SJ, Chappell MA. Optimal sampling schedule for chemical exchange saturation transfer. Magn Reson Med 2013; 70: 1251–62.

Tietze A, Blicher J, Mikkelsen IK, Ostergaard L, Strother MK, Smith SA, et al. Assessment of ischemic penumbra in patients with hyperacute stroke using amide proton transfer (APT) chemical exchange saturation transfer (CEST) MRI. NMR Biomed 2014; 27: 163–74.

van Gelderen P, de Zwart JA, Duyn JH. Pittfalls of MRI measurement of white matter perfusion based on arterial spin labeling. Magn Reson Med 2008; 59: 788–95.

Wintermark M, Albers GW, Broderick JP, Demchuk AM, Fiebach JB, Fiehler J, et al. Acute stroke imaging research roadmap II. Stroke 2013; 44: 2628–39.

Zhang Y, Brady M, Smith S. Segmentation of brain MR images through a hidden Markov random field model and the expectation-maximization algorithm. IEEE Trans Med Imaging 2001; 20: 45–57.

Zhao X, Wen Z, Huang F, Lu S, Wang X, Hu S, et al. Saturation power dependence of amide proton transfer image contrasts in human brain tumors and strokes at 3 T. Magn Reson Med 2011; 66: 1033–41.

Zhou J, Payen JF, Wilson DA, Traystman RJ, van Zijl PC. Using the amide proton signals of intracellular proteins and peptides to detect pH effects in MRI. Nat Med 2003; 9: 1085–90.

Zhou J, van Zijl PC. Defining an acidosis-based ischemic penumbra from pH-weighted MRI. Transl Stroke Res 2011; 3: 76–83.